

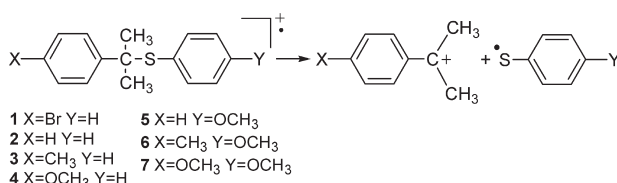
Structure and C–S Bond Cleavage in Aryl 1-Methyl-1-arylethyl Sulfide Radical Cations

Enrico Baciocchi,[†] Marta Bettoni,[‡] Tiziana Del Giacco,[‡] Osvaldo Lanzalunga,^{*,†} Marco Mazzonna,[†] and Paolo Mencarelli[†]

[†]Dipartimento di Chimica and Istituto CNR di Metodologie Chimiche-IMC, Sezione Meccanismi di Reazione c/o Dipartimento di Chimica, Università di Roma La Sapienza, P.le A. Moro 5, 00185 Rome, Italy, and [‡]Dipartimento di Chimica and Centro di Eccellenza Materiali Innovativi Nanostrutturati, Università di Perugia, via Elce di Sotto 8, 06123 Perugia, Italy

osvaldo.lanzalunga@uniroma1.it

Received October 21, 2010



Steady state and laser flash photolysis (LFP) of a series of *p*-X-cumyl phenyl sulfides (4-X-C₆H₄C(CH₃)₂SC₆H₅; **1**, X = Br; **2**, X = H; **3**, X = CH₃; **4**, X = OCH₃) and *p*-X-cumyl *p*-methoxyphenyl sulfides (4-X-C₆H₄C(CH₃)₂SC₆H₄OCH₃; **5**, X = H; **6**, X = CH₃; **7**, X = OCH₃) has been carried out in the presence of *N*-methoxy phenanthridinium hexafluorophosphate (MeOP⁺PF₆[−]) under nitrogen in MeCN. Steady state photolysis showed the formation of products deriving from the C–S bond cleavage in the radical cations **1**^{•+}–**7**^{•+} (2-aryl-2-propanols and diaryl disulfides). Formation of **1**^{•+}–**7**^{•+} was also demonstrated by LFP experiments evidencing the absorption bands of the radical cations **1**^{•+}–**3**^{•+} (λ_{max} = 530 nm) and **5**^{•+}–**7**^{•+} (λ_{max} = 570 nm) mainly localized in the arylsulfenyl group and radical cation **4**^{•+} (λ_{max} = 410, 700 nm) probably mainly localized in the cumyl ring. The radical cations decayed by first-order kinetics with a process attributable to the C–S bond cleavage. On the basis of DFT calculations it has been suggested that the conformations most suitable for C–S bond cleavage in **1**^{•+}–**4**^{•+} and **7**^{•+} are characterized by having the C–S bond almost collinear with the π system of the cumyl ring and by a significant charge and spin delocalization from the ArS ring to the cumyl ring. Such a delocalization is probably at the origin of the observation that the rates of C–S bond cleavage result in very little sensitivity to changes in the C–S bond dissociation free energy (BDFE). A quite large reorganization energy value (λ = 43.7 kcal mol^{−1}) has been calculated for the C–S bond scission reaction in the radical cation. This value is much larger than that (λ = 12 kcal mol^{−1}) found for the C–C bond cleavage in bicumyl radical cations, a reaction that also leads to cumyl carbocations.

Introduction

The chemistry of sulfur radical cations has continued to attract considerable interest, both for the practical and

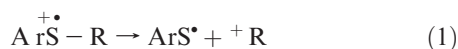
theoretical aspects as well as for the important biological implications.¹ Among the reactions of sulfur radical cations, C–S fragmentation to form an alkyl cation and a sulfenyl radical (eq 1, for the most common case of aromatic sulfides) is one of the most studied decomposition pathways of these species.^{2,3} These reactions represent also an important tool as the detection of fragmentation products can provide

(1) (a) Filipiak, P.; Hug, G. L.; Carmichael, I.; Korzeniowska-Sobczuk, A.; Bobrowski, K.; Marciniak, B. *J. Phys. Chem. A* **2004**, *108*, 6503. (b) Huang, M. L.; Rauk, A. *J. Phys. Chem. A* **2004**, *108*, 6222. (c) Schöneich, C.; Pogocki, D.; Hug, G. L.; Bobrowski, K. *J. Am. Chem. Soc.* **2003**, *125*, 13700. (d) Schöneich, C. *Arch. Biochem. Biophys.* **2002**, *397*, 370. (e) Butterfield, D. A.; Kanski, J. *Peptides* **2002**, *23*, 1299. (f) Korzeniowska-Sobczuk, A.; Hug, G. L.; Carmichael, I.; Bobrowski, K. *J. Phys. Chem. A* **2002**, *106*, 9251. (g) Gawandi, V. B.; Mohan, H.; Mittal, J. P. *J. Phys. Chem. A* **2000**, *104*, 11877. (h) Bonifacici, M.; Hug, G. L.; Schöneich, C. *J. Phys. Chem. A* **2000**, *104*, 1240. (i) Glass, R. S. *Top. Curr. Chem.* **1999**, *205*, 1. (j) Yokoi, H.; Hatta, A.; Ishiguro, K.; Sawaki, Y. *J. Am. Chem. Soc.* **1998**, *120*, 12728. (k) Miller, B. L.; Kucera, K.; Schöneich, C. *J. Am. Chem. Soc.* **1998**, *120*, 3345. (l) Fasani, E.; Freccero, M.; Mella, M.; Albin, A. *Tetrahedron* **1997**, *53*, 2219. (m) Mohan, H.; Mittal, J. P. *J. Phys. Chem. A* **1997**, *101*, 10012. (n) Miller, B. L.; Williams, T. D.; Schöneich, C. *J. Am. Chem. Soc.* **1996**, *118*, 11014. (o) Goetz, M.; Rozwadowski, J.; Marciniak, B. *J. Am. Chem. Soc.* **1996**, *118*, 2882.

(2) (a) Peññory, A. B.; Argüello, J. E.; Puiatti, M. *Eur. J. Org. Chem.* **2005**, *10*, 114. (b) Adam, W.; Argüello, J. E.; Peññory, A. B. *J. Org. Chem.* **1998**, *63*, 3905. (c) Ioele, M.; Steenken, S.; Baciocchi, E. *J. Phys. Chem. A* **1997**, *101*, 2979. (d) Baciocchi, E.; Lanzalunga, O.; Malandrucchio, S.; Ioele, M.; Steenken, S. *J. Am. Chem. Soc.* **1996**, *118*, 8973. (e) Baciocchi, E.; Rol, C.; Scamosci, E.; Sebastiani, G. V. *J. Org. Chem.* **1991**, *56*, 5498.

(3) A sulfide radical cation can also undergo C–S bond cleavage giving a sulfenyl cation and an alkyl radical, but as far as we know, there is no report dealing with this type of cleavage that generally is less thermodynamically favored with respect to that reported in eq 1.

cleancut information on whether radical cations are formed as intermediates in chemical and biological oxidations of sulfur compounds.⁴

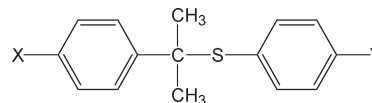


When the SOMO is mostly located on sulfur (eq 1), the cleavage of the C–S bond in a sulfide radical cation presents quite peculiar characteristics with respect to the electronic reorganization connected with the cleavage itself, which differ somewhat from those exhibited by the more intensively investigated C–H, C–C, and C–Si bond cleavages in aromatic radical cations.⁵ In the latter cases the scissile bond is β with respect to the SOMO, which is delocalized in the aromatic ring (β -fragmentation), whereas in the sulfide radical cation the cleaved C–S bond is α to the SOMO on the sulfur atom (α -fragmentation).

Our research group has been long involved in the chemistry of sulfide radical cations, and recently we have focused our attention on the quantitative aspects of reaction (1) in *tert*-alkyl phenyl sulfide radical cations ($\text{PhSCR}_3^{\bullet+}$) through a laser photolysis study.⁶ An interesting observation was that the fragmentation rate depends to a very limited extent on the strength of the C–S bond in the radical cation and that the reorganization energy of the process is influenced by the structure of the alkyl groups. However, this study involved CR_3 groups with different steric hindrance, and the results suggested that steric effects might play a significant role on the rate of the fragmentation process.

Thus, we have felt that the investigation of a series of sulfide radical cations presenting the same steric situation at the scissile bond might give clearer information on the electronic effects on the rate of C–S bond cleavage, and accordingly we now report on a steady state and laser photolysis study of the C–S bond cleavage of the radical cations of a series of aryl cumyl sulfides *para*-substituted in the cumyl ring (**1**–**7**). This study was integrated by DFT calculations at the B3P86/6-311+G(d,p) level of theory for sulfides **1**–**7**, which provided us the C–S bond dissociation energy values (BDEs) that have been used to determine the bond dissociation free energies (BDFEs) in the corresponding

radical cations **1**^{•+}–**7**^{•+}. DFT calculations at the B3LYP/6-311G(d,p) level of theory have been also carried out for radical cations **1**^{•+}–**4**^{•+} and **7**^{•+} in order to get information on the geometry of the radical cations and more importantly on their charge and spin distribution. This information was deemed to be necessary in order to reach a deeper insight on the dynamics of the fragmentation process and particularly on the SOMO location,

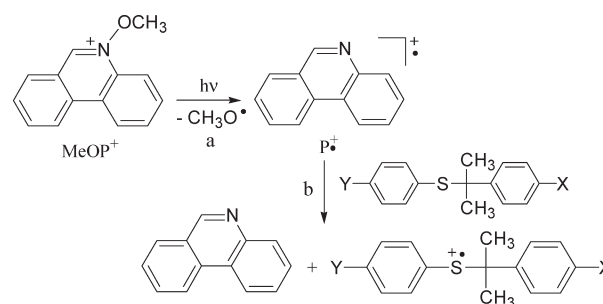


- | | |
|----------|---------------------------------------|
| 1 | X=Br Y=H |
| 2 | X=H Y=H |
| 3 | X=CH ₃ Y=H |
| 4 | X=OCH ₃ Y=H |
| 5 | X=H Y=OCH ₃ |
| 6 | X=CH ₃ Y=OCH ₃ |
| 7 | X=OCH ₃ Y=OCH ₃ |

Results

The method used for the photochemical generation of radical cations **1**^{•+}–**7**^{•+} was the same reported previously for the generation of **2**^{•+}⁶ and is based on the light-induced N–O bond cleavage in the *N*-methoxyphenanthridinium cation (MeOP^+).⁷ The phenanthridinium radical cation ($\text{P}^{\bullet+}$) formed is a quite powerful oxidant ($E^\circ = 1.9$ V vs SCE) able to oxidize the aromatic sulfides, which are characterized by oxidation potentials around or lower than 1.6 V vs SCE^{2c,8} (Scheme 1).

SCHEME 1. Photochemical Generation of Radical Cations **1**^{•+}–**7**^{•+} by MeOP^+



Steady-State Photolysis. Steady state photolysis experiments were carried out by irradiating a solution of sulfides **1**–**7** (0.01 M) in N_2 -saturated CD_3CN at around 355 nm, in the presence of $\text{MeOP}^+\text{PF}_6^-$ (5×10^{-3} M). Reaction products were identified and quantitated by ^1H NMR (products from the alkyl moiety) and GC (sulfur-containing products) analysis, by comparison with authentic specimens. No products were detected without irradiation or in the absence of the sensitizer.

The photolysis of sulfides **1**–**7** produced in substantial amounts the fragmentation products diphenyl disulfide (photooxidation of **1**–**4**) and bis-4-methoxyphenyl disulfide (photooxidation of **5**–**7**) from the sulfide moiety and 2-aryl-2-propanols from the cumyl group. Other products observed

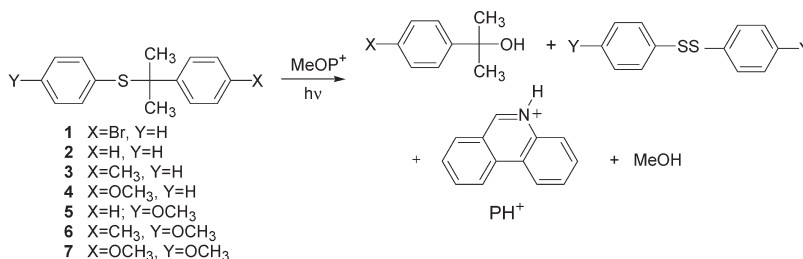
(4) (a) Baclocchi, E.; Del Giacco, T.; Elisei, F.; Lapi, A. *J. Org. Chem.* **2006**, *71*, 853–860. (b) Baclocchi, E.; Del Giacco, T.; Elisei, F.; Gerini, M. F.; Lapi, A.; Liberali, P.; Uzzoli, B. *J. Org. Chem.* **2004**, *69*, 8323. (c) Baclocchi, E.; Lanzalunga, O.; Pirozzi, B. *Tetrahedron* **1997**, *53*, 12287–12298. (d) Baclocchi, E.; Lanzalunga, O.; Marconi, F. *Tetrahedron Lett.* **1994**, *35*, 9771–9774.

(5) (a) Baclocchi, E.; Bietti, M.; Lanzalunga, O. *J. Phys. Org. Chem.* **2006**, *19*, 467–478. (b) Wang, L.; Seiders, J. R.; Floreancig, P. E. *J. Am. Chem. Soc.* **2004**, *126*, 12596–12603. (c) Seiders, J. R.; Wang, L.; Floreancig, P. E. *J. Am. Chem. Soc.* **2003**, *125*, 2406–2407. (d) Kumar, V. S.; Floreancig, P. E. *J. Am. Chem. Soc.* **2001**, *123*, 3842–3843. (e) Baclocchi, E.; Bietti, M.; Lanzalunga, O. *Acc. Chem. Res.* **2000**, *33*, 243. (f) Schmitt, M.; Burghart, A. *Angew. Chem., Int. Ed. Engl.* **1997**, *36*, 2550–2589. (g) Dinnocenzo, J. P.; Simpson, T. R.; Zuilhof, H.; Todd, W. P.; Heinrich, T. *J. Am. Chem. Soc.* **1997**, *119*, 987–993. (h) Dockery, K. P.; Dinnocenzo, J. P.; Farid, S.; Goodman, J. L.; Gould, I. R.; Todd, W. P. *J. Am. Chem. Soc.* **1997**, *119*, 1876–1883. (i) Schepp, N. P.; Shukla, D.; Johnston, L. J.; Sarker, H.; Bauld, N. L. *J. Am. Chem. Soc.* **1997**, *119*, 10325–10334. (j) Gaillard, E. R.; Whitten, D. G. *Acc. Chem. Res.* **1996**, *29*, 292. (k) Maslak, P. *Top. Curr. Chem.* **1993**, *168*, 1. (l) Todd, W. P.; Dinnocenzo, J. P.; Farid, S.; Goodman, J. L.; Gould, I. R. *Tetrahedron Lett.* **1993**, *34*, 2863–2866. (m) Albini, A.; Fasani, E.; d'Alessandro, N. *Coord. Chem. Rev.* **1993**, *125*, 269. (n) Popielarz, R.; Arnold, D. R. *J. Am. Chem. Soc.* **1990**, *112*, 3068–3082. (o) Dinnocenzo, J. P.; Farid, S.; Goodman, J. L.; Gould, I. R.; Todd, W. P.; Mattes, S. L. *J. Am. Chem. Soc.* **1989**, *111*, 8973–8975.

(6) Baclocchi, E.; Del Giacco, T.; Gerini, M. F.; Lanzalunga, O. *Org. Lett.* **2006**, *8*, 641–644.

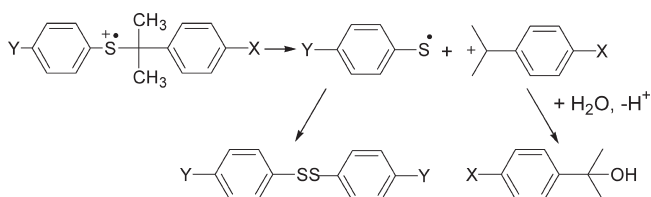
(7) Shukla, D.; Guanghua, L.; Dinnocenzo, J. P.; Farid, S. *Can. J. Chem.* **2003**, *81*, 744.

(8) Baclocchi, E.; Crescenzi, C.; Lanzalunga, O. *Tetrahedron* **1997**, *53*, 4469.

SCHEME 2. Fragmentation Products in the Photooxidation of Sulfides 1–7 by MeOP⁺

were those deriving from the N–O fragmentation of the MeOP⁺ (protonated phenanthridine, PH⁺ and methanol) (Scheme 2).

The structure of photoproducts formed can reasonably be rationalized on the basis of the formation of the radical cations 1^{•+}–7^{•+} followed by the unimolecular cleavage of the C–S bond (eq 1). This process leads to the 1-methyl-1-arylethyl cations and the arylsulfenyl radicals (Scheme 3).⁹ The cations can then react with water¹¹ to form the alcohols. Dimerization of arylsulfenyl radicals leads to diaryl disulfides.

SCHEME 3. C–S Bond Cleavage of Radical Cations 1^{•+}–7^{•+}

In the photooxidation of **4** and **7**, 2-(4-methoxyphenyl)-2-propanol was accompanied by significant amounts of two dimeric products: 2,4-bis(4-methoxyphenyl)-4-methyl-2-pentene (**8**) and 2,4-bis(4-methoxyphenyl)-4-methyl-1-pentene (**9**). As reported in the literature,¹² these products likely form because the 2-(4-methoxyphenyl)-2-propyl carbocation produced after C–S bond cleavage in 4^{•+} and 7^{•+} is relatively stable, and thus the reaction with water to give 2-(4-methoxyphenyl)-2-propanol occurs in competition with other processes (deprotonation to give 2-(4-methoxyphenyl)-propene followed by coupling with a second molecule of carbocation) leading to the two dimeric products as shown in Scheme 4.

The quantum yields (Φ) measured for the products are reported in Table 1. As expected, the quantum yields (Φ) of diaryl disulfides (Table 1) are about half of that of the products deriving from the cumyl moiety.

Laser Flash Photolysis Studies. By laser photolysis ($\lambda_{\text{exc}} = 355$ nm) of N₂-saturated CH₃CN solutions of sulfides **1**–**3** (0.01 M) and MeOP⁺ (1.6×10^{-4} M), a broad and intense absorption with maximum around 530 nm, accompanied by a less intense absorption centered at 390 nm were detected after the laser pulse. As an example, the time-resolved spectra

of the LFP experiment with the **3**/MeOP⁺ system are reported in Figure 1. The results of the LFP experiments with the MeOP⁺/**2** system (already reported in a previous study⁶) and with the **1**/MeOP⁺ system are shown in Figures S1–S2 in the Supporting Information.

The intense absorption band at 530 nm can be assigned to the radical cations 1^{•+}–3^{•+},^{6,13} formed by oxidation of sulfides **1**–**3** by the phenanthridine radical cation (P^{•+}) produced after N–O bond fragmentation in the MeOP⁺ excited state.⁶ Time-resolved absorption spectra are not modified by the presence of oxygen, thus confirming the cationic nature of the transients.

The time-evolution of the absorption spectra showed a slow first-order decay of the signal at 530 nm (see inset of Figure 1) substantially coupled with the growth of the absorption at around 380–390 nm that can reasonably be attributed to the formation of the 4-X-C₆H₄C(CH₃)₂⁺ cations ($\lambda_{\text{max}} = 380$ –410 nm).¹⁴ This observation confirms the results of steady-state photolysis suggesting a decay of 1^{•+}–3^{•+} due to the C–S bond cleavage with formation of 1-methyl-1-arylethyl cations and the phenylsulfenyl radical C₆H₅S[•]. The latter species does not emerge in the spectra because its low extinction coefficient.¹⁵

While results of the time-resolved spectra of the MeOP⁺/**1**–**3** systems were very similar, different features were observed in the time-resolved spectra of the MeOP⁺/**4** system. Upon laser excitation of a solution of MeOP⁺ (1.6×10^{-4} M) and **4** (1.0×10^{-2} M) in N₂-saturated CH₃CN, an absorption band at 410 nm was detected just after the laser pulse accompanied by a broad band in the near-infrared (NIR) region of the spectrum ($\lambda > 650$ nm) (Figure 2).

The 410 nm band is significantly blue-shifted with respect to the absorption bands of radical cations 1^{•+}–3^{•+}, and its assignment is more in accordance with a radical cation mostly localized in the methoxylated cumyl ring. This hypothesis is supported by the presence of the band in the NIR region of the spectrum that can be assigned to an intramolecular charge resonance interaction between the neutral phenylsulfenyl ring and the charged acceptor 4-methoxylated cumyl ring.¹⁶ In agreement, theoretical calculations

(13) Baclocchi, E.; Del Giacco, T.; Giombolini, P.; Lanzalunga, O. *Tetrahedron* **2006**, 62, 6566–6573.

(14) McClelland, R. A.; Chan, C.; Cozens, F. L.; Modro, A.; Steenken, S. *Angew. Chem., Int. Ed. Engl.* **1991**, 30, 1337.

(15) λ_{max} (C₆H₅S[•]) = 460 nm, $\epsilon = 2.6 \times 10^3$ M^{−1} s^{−1}. Tripathi, G. N. R.; Sun, Q.; Armstrong, D. A.; Chipman, D. M.; Schuler, R. H. *J. Phys. Chem.* **1992**, 96, 5344.

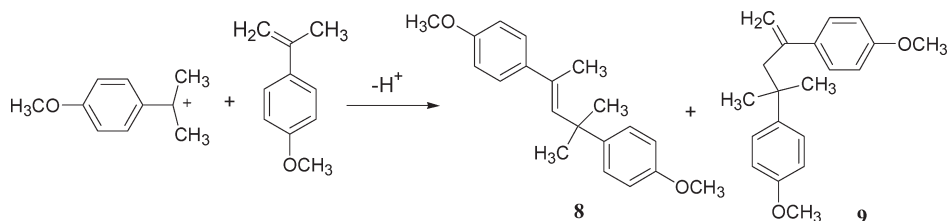
(16) Intramolecular charge resonance interaction between a charged acceptor methoxylated aromatic radical cation and neutral donor aromatic rings in diarylmethanol radical cations^{17a} and in trimeric lignin model compounds^{17b} led to absorption bands in the NIR region of the spectrum similar to that observed in 4^{•+}.

(9) The C–S cleavage occurs by a unimolecular pathway as demonstrated by the study of the stereochemistry of the C–S fragmentation in 1-phenylethyl phenyl sulfide radical cation.¹⁰

(10) Baclocchi, E.; Fasella, E.; Lanzalunga, O.; Mattioli, M. *Angew. Chem., Int. Ed. Engl.* **1993**, 32, 1071–1073.

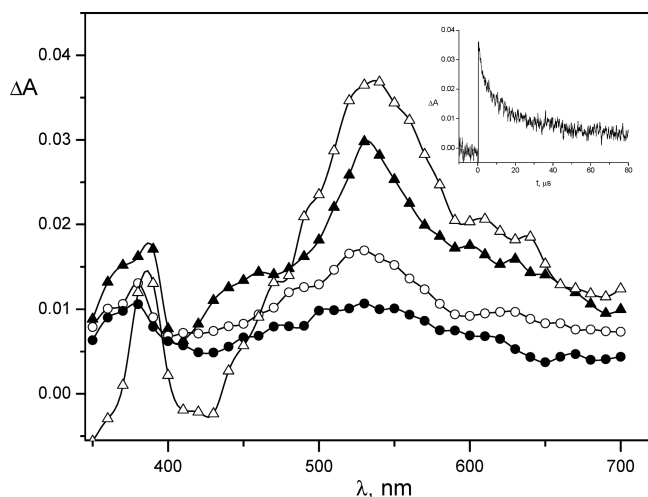
(11) The water content was ca. 0.01 M in the spectrophotometric grade CH₃CN used in all of the experiments

(12) Del Giacco, T.; Faltoni, A.; Elisei, F. *Phys. Chem. Chem. Phys.* **2008**, 10, 200–210.

SCHEME 4. Formation of Dimeric Products in the Photooxidation of Sulfides **4** and **7** by MeOP⁺TABLE 1. Quantum Yields (Φ) of Products Formed in the Photooxidation of Aryl 1-Methyl-1-arylethyl Sulfides (**1**–**7**) Sensitized by MeOP⁺ in N₂-Saturated CD₃CN^a

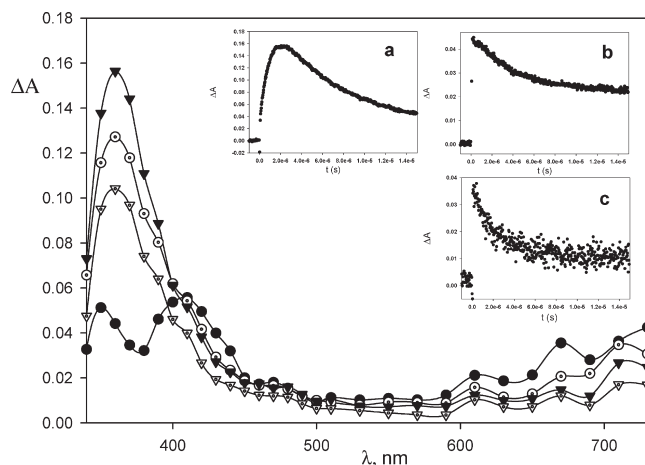
Sulfide	Fragmentation Products (Φ)		
		Dimers 8-9	
1	0.45	-	0.24
2	0.79	-	0.42
3	0.58	-	0.32
4	0.18	0.27	0.33
5	0.55	-	0.30
6	0.62	-	0.35
7	0.06	0.36	0.38

^a[sulfide] = 1.0×10^{-2} M, [MeOP⁺] = 5.0×10^{-3} M under nitrogen. The error is $\pm 10\%$.

FIGURE 1. Time-resolved absorption spectra of the MeOP⁺ (1.6×10^{-4} M)/4-CH₃C₆H₄C(CH₃)₂SC₆H₅ (**3**) (1.0×10^{-2} M) system in N₂-saturated CH₃CN recorded 0.2 (Δ), 2.4 (\blacktriangle), 7.4 (\circ) and 16 (\bullet) μ s after the laser pulse. Inset: decay kinetics recorded at 530 nm.

have shown that in **4**⁺ the charge and spin densities are more localized in the cumyl ring than in the ArS ring (vide infra).

The time-evolution of the absorption spectra shows that the signal decay recorded at 420 nm (Figure 2, inset b) and 700 nm (Figure 2, inset c) is coupled with the growth of an

FIGURE 2. Time-resolved absorption spectra of the MeOP⁺ (1.6×10^{-4} M)/4-CH₃OC₆H₄C(CH₃)₂SC₆H₅ (**4**) (1.0×10^{-2} M) system in N₂-saturated CH₃CN recorded 96 ns (\bullet), 0.9 μ s (\circ), 2.0 μ s (\blacktriangledown), and 5.9 μ s (∇) after the laser pulse. Insets: (a) buildup and decay kinetics recorded at 360 nm; (b) decay kinetics recorded at 420 nm; (c) decay kinetics recorded at 700 nm.

absorption band centered at 360 nm (Figure 2, inset a). This band can be reasonably attributed to the 4-methoxycumyl cation 4-CH₃OC₆H₄C(CH₃)₂⁺ in accordance with the spectrum reported in the literature ($\lambda_{\text{max}} = 360$ nm).¹⁴ The nature of this transient is confirmed by the fact that addition of small amounts of water leads to a significant increase of its decay rate.¹⁸

LFP experiments with the MeOP⁺/5–7 systems led to results similar to those found with the MeOP⁺/1–3 systems. Solutions of the methoxylated sulfides **5**–**7** (0.01 M) and MeOP⁺ (1.6×10^{-4} M), after the laser pulse, exhibited a broad and intense absorption with maximum around 570 nm, accompanied by a less intense absorption centered at 390 nm. The time-resolved spectra are reported in Figures S3–S5 in Supporting Information. The intense absorption band at 570 nm can be assigned to the radical cations **5**^{•+}–**7**^{•+}¹⁹ formed by oxidation of sulfides **5**–**7** by the phenanthridine radical cation (P^{•+}).

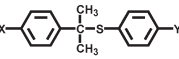
The time-evolution of the absorption spectra showed a first-order decay of the signal at 570 nm (see inset of Figures S3–S5 in Supporting Information) slower than that observed in the LFP experiment with the corresponding non-methoxylated cumyl sulfides **2**–**4**. Again the decay was

(18) The decay rate increase from 8.6×10^4 s^{−1} in the absence of water to 7.2×10^5 s^{−1} in the presence of 0.4% (v/v) of water. The rate of decay of 4-CH₃OC₆H₄C(CH₃)₂⁺ in 2:1 (v/v) water/CH₃CN is 4×10^7 s^{−1}.¹⁴

(19) A similar λ_{max} value (580 nm) has been reported for the radical cation of 4-methoxythioanisole in water. Jonsson, M.; Lind, J.; Merényi, G.; Eriksen, T. E. *J. Chem. Soc., Perkin Trans. 2* **1995**, 67–70.

(17) (a) Bietti, M.; Lanzalunga, O. *J. Org. Chem.* **2002**, 67, 2632. (b) Baclocchi, E.; Fabbri, C.; Lanzalunga, O. *J. Org. Chem.* **2003**, 68, 9061–9069.

TABLE 2. Decay Rate Constants (k_f) of Aryl 1-Methyl-1-arylethyl Sulfide Radical Cations (1^{+*} – 7^{+*}) Generated by Photooxidation of 1–7 Sensitized by MeOP⁺PF₆[−] ($\lambda_{\text{exc}} = 355$ nm), Oxidation Peak Potentials (E_p), and C–S Bond Dissociation Energies (BDEs) for the Sulfides 1–7 and C–S Bond Dissociation Free Energies (BDFEs) for Radical Cations 1^{+*} – 7^{+*}

	$k_f (10^5 \text{ s}^{-1})^a$	E_p^b	C–S BDE (neutral substrates) ^{c,d}	C–S BDFE (radical cations) ^{d,e,f}
1^{+*} X=Br Y=H	0.36	1.60	42.0	0.4
2^{+*} X=H Y=H	0.45	1.56	42.3	0.1
3^{+*} X=CH ₃ Y=H	0.58	1.55	42.3	-2.9
4^{+*} X=OCH ₃ Y=H	4.5	1.49	42.5	-5.1
5^{+*} X=H Y=OCH ₃	< 0.1	1.31	39.9	3.4
6^{+*} X=CH ₃ Y=OCH ₃	< 0.1	1.31	39.9	-0.1
7^{+*} X=OCH ₃ Y=OCH ₃	0.47	1.32	40.1	-3.6

^aFrom LFP experiments in N₂-saturated CH₃CN. [sulfide] = 1.0×10^{-2} M, [MeOP⁺PF₆[−]] = 8.8×10^{-4} M. ^bOxidation peak potential in V vs SCE in CH₃CN. ^cFrom DFT calculations, see text. ^dkcal mol^{−1}. ^eAt 298 K. ^fDetails of calculations in Supporting Information

accompanied by a growth of absorption at 380–400 nm due to the formation of 1-methyl-1-arylethyl cations. In the time-resolved spectra of the MeOP⁺/7 system at longer delay times an absorption peak centered at 525 nm is observed (see Figure S5 in Supporting Information) which can be assigned to 4-CH₃OC₆H₄S[•] according to the literature.²⁰ In this case the decay rate of 7^{+*} is fast enough (vide infra) to allow the observation of the sulfenyl radical.²¹

It can be noted that in the MeOP⁺/7 LFP experiment the band at 360 nm attributed to 4-CH₃OC₆H₄C(CH₃)₂⁺ is less intense than that observed in the LFP experiment with MeOP⁺/4. This is likely due to the fact that when produced from fragmentation of 4^{+*} the formation of 4-CH₃OC₆H₄C(CH₃)₂⁺ ($k_{\text{buildup}} \approx 1.6 \times 10^6 \text{ s}^{-1}$, see inset a of Figure 2) is faster than its decay ($k_{\text{decay}} \approx 8.6 \times 10^4 \text{ s}^{-1}$), whereas the opposite occurs when 4-CH₃OC₆H₄C(CH₃)₂⁺ is produced from C–S bond cleavage in 7^{+*} .

The decay rates of the radical cations were determined by following the kinetics at 530 nm for 1^{+*} – 3^{+*} , at 570 nm for 5^{+*} – 7^{+*} and at 700 nm for 4^{+*} (insets of Figures 1 and 2 and S1–S5 in Supporting Information). In all cases the decay kinetics followed first order laws in accordance with the unimolecular fragmentation process.^{9,22} The rate of fragmentation of 5^{+*} and 6^{+*} were too low, and only an upper limit rate constant ($k_f < 1 \times 10^4 \text{ s}^{-1}$) has been given for these processes. The rate constants (k_f) measured at 25 °C are reported in Table 2.

Theoretical Calculations. Neutral Sulfides. For a meaningful discussion of the experimental results, it was necessary

to know the C–S bond dissociation free energies (BDFEs) for the sulfide radical cations 1^{+*} – 7^{+*} . These values were estimated by the usual thermochemical cycle⁶ (details in Supporting Information) using the C–S BDEs for the neutral sulfides 1–7 obtained by DFT calculations, carried out by using the Gaussian 03 package,²³ at the B3P86/6-311+G(d,p)//B3P86/6-311+G(d,p) level of theory. The B3P86 functional was chosen because it is reported to be applied with reasonable success to the calculations of BDE values for a variety of C–X bonds,^{24,25} including C–S bonds.²⁵ It should also be noted that even though DFT methods may underestimate absolute BDE values, this should not affect the relative BDE values,^{25c} which are those we are mostly concerned with. The calculated C–S BDEs of 1–7 are reported in Table 2 together with the BDFEs of the corresponding radical cations obtained by the thermochemical cycle using the C–S BDEs for the neutral sulfides 1–7 corrected for the entropic factor, the peak oxidation potentials of the sulfides reported in Table 2, and the reduction potentials of the leaving carbocations available from the literature.²⁶

Since we are dealing with conformationally flexible molecules, before starting the BDEs calculation, all available conformations for the molecule and the radicals formed in the C–S scission process have to be found. To this end, a systematic conformational search was carried out, at the semiempirical PM3 level of theory,²⁷ by using the Conformer Search Module available in the Spartan 5.01 package.²⁸ All of the conformers found were optimized again, first at the B3LYP/6-31G level of theory and then at the higher B3P86/6-311+G(d,p) level of theory. The number of conformers found for sulfides 1–7 were two for 1, two for 2, two for 3, four for 4, four for 5, four for 6, and eight for 7. Only one conformer was found for each radical fragment.

In all of the calculations, the keywords integral (grid = ultrafine) scf = tight were used. For open shell (radical) species, spin contamination due to states of multiplicity higher than the doublet state was negligible since the

(20) Darmanyan, A. P.; Gregory, D. D.; Guo, Y.; Jencks, W. S. *J. Phys. Chem. A* **1997**, *101*, 6855–6863.

(21) The absorption spectrum of 4-CH₃OC₆H₄S[•], obtained by laser photolysis of *tert*-butylperoxide (0.4 M) in the presence of 4-CH₃OC₆H₄SH (2.7×10^{-2} M) in MeCN, shows a broad band centered at 520 nm (shoulder at 470 nm). This transient decays by second-order kinetics with $t_{1/2} = 7.3 \mu\text{s}$.

(22) The radical cation decays were somewhat complicated by the presence of a transient species as already found by Dinnocenzo et al.⁷ The decay rate constant for this species was the same in all samples (ca. $1 \times 10^6 \text{ s}^{-1}$), and the nature of this transient has not been identified even though it is likely due to the photolysis of MeOP⁺.

(23) Frisch, M. J.; Trucks, G. W.; Schlegel, H. B.; Scuseria, G. E.; Robb, M. A.; Cheeseman, J. R.; Montgomery, Jr., J. A.; Vreven, T.; Kudin, K. N.; Burant, J. C.; Millam, J. M.; Iyengar, S. S.; Tomasi, J.; Barone, V.; Mennucci, B.; Cossi, M.; Scalmani, G.; Rega, N.; Petersson, G. A.; Nakatsuji, H.; Hada, M.; Ehara, M.; Toyota, K.; Fukuda, R.; Hasegawa, J.; Ishida, M.; Nakajima, T.; Honda, Y.; Kitao, O.; Nakai, H.; Klene, M.; Li, X.; Knox, J. E.; Hratchian, H. P.; Cross, J. B.; Adamo, C.; Jaramillo, J.; Gomperts, R.; Stratmann, R. E.; Yazyev, O.; Austin, A. J.; Cammi, R.; Pomelli, C.; Ochterski, J. W.; Ayala, P. Y.; Morokuma, K.; Voth, G. A.; Salvador, P.; Dannenberg, J. J.; Zakrzewski, V. G.; Dapprich, S.; Daniels, A. D.; Strain, M. C.; Farkas, O.; Malick, D. K.; Rabuck, A. D.; Raghavachari, K.; Foresman, J. B.; Ortiz, J. V.; Cui, Q.; Baboul, A. G.; Clifford, S.; Cioslowski, J.; Stefanov, B. B.; Liu, G.; Liashenko, A.; Piskorz, P.; Komaromi, I.; Martin, R. L.; Fox, D. J.; Keith, T.; Al-Laham, M. A.; Peng, C. Y.; Nanayakkara, A.; Challacombe, M.; Gill, P. M. W.; Johnson, B.; Chen, W.; Wong, M. W.; Gonzalez, C.; Pople, J. A. *Gaussian 03, Revision B.05*; Gaussian, Inc.: Pittsburgh, PA, 2003.

(24) (a) Yao, X.-Q.; Hou, X.-J.; Jiao, H.; Wu, G.-S.; Xu, Y.-Y.; Xiang, H.-W.; Jiao, H.; Li, Y.-W. *J. Phys. Chem. A* **2002**, *106*, 7184. (b) Zhao, J.; Cheng, X.; Yang, X. *J. Mol. Struct. (Theochem)* **2006**, *766*, 87. (c) Van Speybroeck, V.; Marin, G. B.; Waroquier, M. *ChemPhysChem* **2006**, *7*, 2205. (d) Su, X.-F.; Cheng, X.; Liu, Y.-G.; Li, Q. *Int. J. Quantum Chem.* **2007**, *107*, 515.

(25) (a) Johnson, E. R.; Clarkin, O. J.; DiLabio, G. A. *J. Phys. Chem. A* **2003**, *107*, 9953. (b) Yao, X.-Q.; Hou, X.-J.; Jiao, H.; Xiang, H.-W.; Li, Y.-W. *J. Phys. Chem. A* **2003**, *107*, 9991. (c) Feng, Y.; Liu, L.; Wang, J.-T.; Huang, H.; Guo, Q.-X. *J. Chem. Inf. Comput. Sci.* **2003**, *43*, 2005.

(26) Sim, B. A.; Milne, H.; Griller, D.; Wayner, D. D. M. *J. Am. Chem. Soc.* **1990**, *112*, 6635–6638.

(27) Stewart, J. J. P. *J. Comput. Chem.* **1989**, *10*, 209.

(28) *Spartan 5.01*; Wavefunction, Inc.: Irvine, CA.

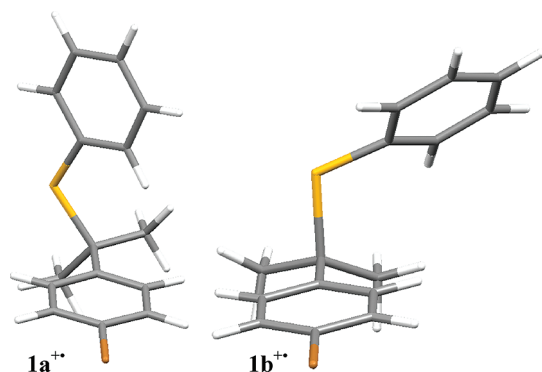


FIGURE 3. 4-BrC₆H₄C(CH₃)₂SC₆H₅¹⁺ conformers at the minimum of energy.

expectation value $\langle S^2 \rangle$ of the total spin operator S^2 was, in all cases, within 5% of the expectation value for a doublet (0.75). Harmonic vibrational frequencies were calculated at the B3P86/6-311+G(d,p) level of theory to confirm that the stationary points found correspond to local minima and to obtain the zero-point vibrational energy (ZPVE) corrections. For the ZPVE a scale factor of 0.9845 was used.²⁹ When more than one conformer was found for a given compound, its energy ($E_{el} + E_{ZPVE}$) to be used in the BDEs calculation, was obtained by Boltzmann averaging the energy ($E_{el} + E_{ZPVE}$) of all of the corresponding minima. In the Supporting Information are reported the Cartesian coordinates, the electronic energy, and the zero-point vibrational energy of all of the minima found.

Sulfide Radical Cations. DFT calculations were performed for those sulfide radical cations characterized by measurable fragmentation rate constants ($1^{+•}$ – $4^{+•}$ and $7^{+•}$) with the aim of obtaining the geometry of the minima, charges, and spin distributions. The calculations were carried out at the B3LYP/6-311G(d,p)//B3LYP/6-311G(d,p) level of theory, the same that was already used in a previous work on similar sulfide radical cations.³⁰

The starting geometries for the energy minimization of each radical cation were those of the corresponding neutral sulfide. Harmonic vibrational frequencies were calculated at the B3LYP/6-311G(d,p) level of theory to confirm that the stationary points found correspond to local minima. For all of the radical cations, spin contamination due to states of multiplicity higher than the doublet state was negligible since the expectation value $\langle S^2 \rangle$ of the total spin operator S^2 was, in all cases, within 5% of the expectation value for a doublet (0.75). Two minima were found for $1^{+•}$ – $4^{+•}$, and eight minima were instead found for $7^{+•}$. The atomic charges were obtained by Natural Population Analysis (NPA).³¹ Unpaired electron spin densities were calculated using the Mulliken population analysis.

The two energy minimum conformations for $1^{+•}$ – $3^{+•}$ ($1a^{+•}$ – $3a^{+•}$ and $1b^{+•}$ – $3b^{+•}$) exhibit quite different geometry, (see later for further details). In Figure 3 are reported the $1a^{+•}$ and $1b^{+•}$ conformers ($2a^{+•}$ – $2b^{+•}$ and $3a^{+•}$ – $3b^{+•}$ conformers are reported in Figures S8 and S9 in the Supporting Information). $1a^{+•}$ is 0.42 kcal/mol lower in energy than $1b^{+•}$

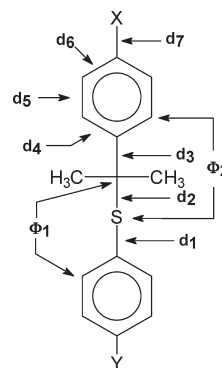


FIGURE 4. Definition of geometrical features of radical cations $1^{+•}$ – $4^{+•}$, $7^{+•}$ reported in Table 3.

TABLE 3. Most Significant Dihedral Angles (deg) and Bond Lengths (Å) of Radical Cations $1^{+•}$ – $4^{+•}$, $7^{+•}$

	Φ_1	Φ_2	d_1	d_2	d_3	$\langle d_4 \rangle$	$\langle d_5 \rangle$	$\langle d_6 \rangle$	d_7
1a	–8	55	1.735	1.908	1.521	1.405	1.389	1.396	1.896
1b	58	90	1.757	1.945	1.512	1.416	1.381	1.402	1.884
2a	–8	54	1.729	1.916	1.522	1.403	1.392	1.394	
2b	53	92	1.751	1.949	1.515	1.415	1.384	1.398	
3a	8	–55	1.736	1.910	1.519	1.405	1.388	1.402	1.503
3b	–60	90	1.759	1.947	1.510	1.418	1.380	1.409	1.498
4a	–69	92	1.770	1.939	1.505	1.421	1.374	1.415	1.325
4b	68	90	1.770	1.939	1.506	1.422	1.373	1.416	1.325
7a	7	–55	1.733	1.913	1.519	1.405	1.386	1.404	1.343
7b	–57	88	1.747	1.960	1.505	1.415	1.378	1.411	1.333

and $2a^{+•}$ is 1.45 kcal/mol lower in energy than $2b^{+•}$, whereas $3a^{+•}$ and $3b^{+•}$ have approximately the same energy.

The two energy minimum conformations for $4^{+•}$ (Figure S10 in Supporting Information) have a similar geometry differing only for the relative orientation of the methoxy group with respect to the phenylsulfenyl group. Both conformations resemble those found for conformers $1b^{+•}$ – $3b^{+•}$ (vide infra).

For radical cation $7^{+•}$ eight energy minimum conformations were found. These conformations can be divided, by the geometrical point of view, in two families resembling the above-mentioned **a** type (four conformations due to the four possible relative orientations of the two methoxy groups) and **b** type (four conformations) for the radical cations $1^{+•}$ – $3^{+•}$ (vide infra). The relative amount of the two types **a** and **b** can be calculated as 74% and 26%, respectively. The most stable of each type of conformation is shown in Figure S11 in the Supporting Information.

The most significant geometrical features (dihedral angles and bond length as defined in Figure 4) of radical cations $1^{+•}$ – $4^{+•}$, $7^{+•}$ are reported in Table 3.

In Table 4 are displayed NPA Charges and spin density values obtained for radical cations in $1^{+•}$ – $4^{+•}$, $7^{+•}$, partitioned for the different structural components of the radical cations defined in Figure 5.

From the data reported in Table 3, it can be observed that the **a** conformations for radical cations $1^{+•}$ – $3^{+•}$ and $7^{+•}$ have very similar geometries, and the same can be said for the **b** conformations, **a** and **b** being however characterized by distinct geometrical features. In particular the dihedral angle Φ_1 is around 8° for the **a** conformers (the fragmenting C–S bond is almost coplanar with the phenylsulfenyl ring as already observed in the minimum energy conformers of alkyl

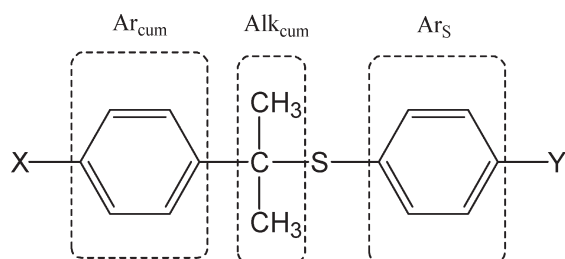
(29) Merrick, J. P.; Moran, D.; Radom, L. *J. Phys. Chem. A* **2007**, *111*, 11683.

(30) Baciacchi, E.; Gerini, M. F. *J. Phys. Chem. A* **2004**, *108*, 2332–2338.

(31) Reed, A. E.; Curtiss, L. A.; Weinhold, F. *Chem. Rev.* **1988**, *88*, 899.

TABLE 4. NPA Charges (q_{NPA}) and Spin Densities for Radical Cations $1^{+\bullet}$ – $4^{+\bullet}$, $7^{+\bullet}$

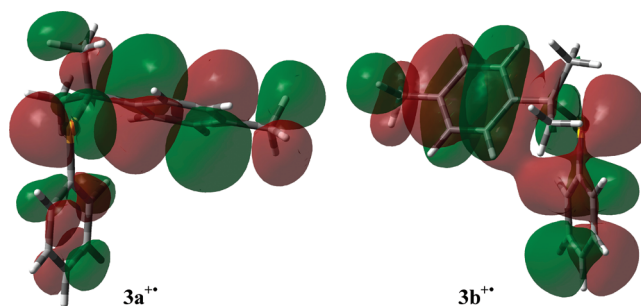
		Ar _{cum}	Alk _{cum}	S	Ar _S	X	Y
1a	q_{NPA}	−0.003	0.060	0.595	0.194	0.154	
1a	spin	0.112	−0.005	0.492	0.362	0.038	
1b	q_{NPA}	0.118	0.071	0.534	0.078	0.200	
1b	spin	0.300	−0.012	0.459	0.175	0.077	
2a	q_{NPA}	0.095	0.068	0.617	0.221		
2a	spin	0.077	−0.002	0.528	0.397		
2b	q_{NPA}	0.251	0.079	0.565	0.105		
2b	spin	0.293	−0.011	0.503	0.215		
3a	q_{NPA}	0.091	0.060	0.598	0.181	0.070	
3a	spin	0.147	−0.006	0.505	0.349	0.005	
3b	q_{NPA}	0.246	0.072	0.535	0.064	0.084	
3b	spin	0.372	−0.011	0.468	0.159	0.013	
4a	q_{NPA}	0.538	0.052	0.473	0.012	−0.075	
4a	spin	0.420	−0.015	0.392	0.090	0.113	
4b	q_{NPA}	0.538	0.053	0.476	0.010	−0.076	
4b	spin	0.421	−0.016	0.394	0.090	0.111	
7a	q_{NPA}	0.289	0.048	0.517	0.372	−0.146	−0.079
7a	spin	0.093	0.002	0.396	0.371	0.028	0.109
7b	q_{NPA}	0.438	0.058	0.450	0.270	−0.107	−0.110
7b	spin	0.292	−0.007	0.356	0.215	0.079	0.065

**FIGURE 5**

phenyl sulfide radical cations³⁰) and 53–60° for the **b** conformers. A difference in the dihedral angle Φ_2 is also observed being around 55° for the **a** conformers and around 90° for the **b** conformers (where the fragmenting C–S bond is almost perpendicular to the cumyl ring). Significant differences in the bond lengths are also observed between the **a** and **b** conformers. In particular the d_2 fragmenting C–S bond and the C–C bonds d_4 and d_6 in the cumyl ring are always longer in the **b** conformers of $1^{+\bullet}$ – $3^{+\bullet}$, $7^{+\bullet}$. On the opposite the C–S bond d_3 and the C–C bond d_5 are always longer in the **a** conformers of $1^{+\bullet}$ – $3^{+\bullet}$, $7^{+\bullet}$. In other words, the cumyl ring in the **b** conformers has a more quinoid-like structure.³²

Interestingly, for $4^{+\bullet}$ the two conformers are instead characterized by a similar geometry resembling that of radical cations $1b^{+\bullet}$ – $3b^{+\bullet}$. The dihedral angles Φ_1 and Φ_2 are in both the conformers close to 70° and 90°, respectively. The bond distances are also practically the same in the two conformations and similar to those found for the **b** conformers of $1^{+\bullet}$ – $3^{+\bullet}$.

From the data reported in Table 4, it can be noted that like the geometries, the distribution of charge and spin density too is significantly different in the **a** and **b** conformations of

**FIGURE 6.** SOMO of the two energy minimum conformers of $3^{+\bullet}$.

cumyl sulfide radical cations $1^{+\bullet}$ – $3^{+\bullet}$. If, for example, we consider the most stable conformer of cumyl phenyl sulfide radical cation $2a^{+\bullet}$, it can be noted that NPA charges and spin populations are mainly localized on the Ar_S ring and on the sulfur atom. On going to conformer $2b^{+\bullet}$ we note that the charge and spin density increase significantly in the Ar_{cum} ring and almost correspondingly decrease in the Ar_S ring, whereas the sulfur atom is little affected.

An increase of charge and spin density on the cumyl ring at the expense of that on the Ar_S ring on going from the **a** to the **b** conformer, is also observed in radical cations $1^{+\bullet}$ – $3^{+\bullet}$ and $7^{+\bullet}$. A reasonable explanation is that in the **b** conformations a through-space interaction between the aromatic rings of the phenylsulfenyl and the cumyl moieties takes place. In other words, the charge and spin density of the radical cation which are mainly localized on the Ar_S ring and sulfur in the **a** conformation (mostly on sulfur) are still mainly localized on sulfur in the **b** conformation, but now there is a significant delocalization between the Ar_{cum} and the Ar_S rings. This specific interaction between the two aromatic rings is well visualized in the SOMO representation for $3b^{+\bullet}$ shown in Figure 6.

This delocalization occurs only in the **b** conformers as in this case the two aromatic systems are almost facing each other (the dihedral angle between the planes of the two rings is 40–53°). In the **a** conformers instead the dihedral angle between the planes of the two aromatic rings (around 90°) does not allow an analogous spin and charge delocalization as shown by the SOMO of $3a^{+\bullet}$ reported in Figure 6. This shift of charge and spin between the two rings can also be represented as a contribution of the resonance structure II to the **b** conformation of the radical cation (Figure 7) more important of that of structure III (the reverse holds in the **a** conformations). It can be noted that the relative stability of the **b** with respect to the **a** conformer in $1^{+\bullet}$ – $3^{+\bullet}$ increases by increasing the +R electron donating power of the X substituent (H < Br < CH₃, higher contribution of the resonance structure II in Figure 7).

A further observation is that in **b** conformations the C–S bond (d_2 in Figure 6) is significantly longer than in **a** conformations and is almost exactly perpendicular to the cumyl ring. These two observations lead us to suggest some hyperconjugative interaction between the d_2 C–S bond and the π system of the cumyl ring, which can be represented by a contribution of structure IV (Figure 7). In view of the very low charge on the Alk_{cum} group (Table 4) we feel, however, that structure IV should be a much less important contributor to the resonance hybrid of **b** conformations of radical cations $1^{+\bullet}$ – $3^{+\bullet}$ and $7^{+\bullet}$ than structure II.

(32) The degree of planarity of the cumyl carbon bonded to the S atom, defined by the difference between 360° and the sum of the CH₃–C–CH₃, CH₃–C–C(Ar_{cum}), and C(Ar_{cum})–C–CH₃ angles, was always higher for the **b** conformers of $1^{+\bullet}$ – $3^{+\bullet}$ with respect to the **a** conformers (see Table S2 in Supporting Information).

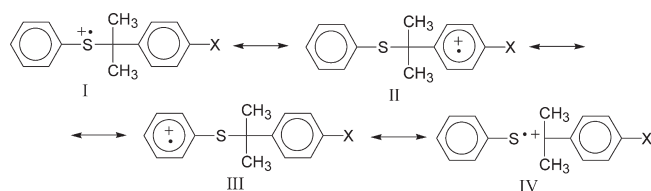


FIGURE 7. Resonance structures for radical cations $1^{+\bullet}$ – $4^{+\bullet}$.

It has been already said that, differently from the other radical cations, with $4^{+\bullet}$ the two conformers $4a^{+\bullet}$ and $4b^{+\bullet}$ have very similar geometries. Analogously, similar values of charge and spin distribution in the Ar_{cum} and Ar_S rings are exhibited by the two conformers. It is noticeable that in both conformations, the presence of the methoxy substituent in the cumyl ring of $4^{+\bullet}$ determines a >0.5 charge distribution in the Ar_{cum} , indicating a predominating role of structure II with this radical cation, whereas that of structure III seems almost negligible. This is in nice agreement with the previously discussed UV–vis spectrum of $4^{+\bullet}$, which has suggested an anisole type radical cation. For radical cation $4^{+\bullet}$ both conformers **a** and **b** show the possibility of a through-space interaction of the phenylsulfenyl ring with the spin and charge densities in the cumyl system that appears significantly enhanced by the presence of the methoxy group.³³ We remind that for radical cations $1^{+\bullet}$ – $3^{+\bullet}$ and $7^{+\bullet}$, instead, UV–vis spectra have suggested a sulfur type radical cation, which is in line with the finding that for these radical cations (particularly for $1^{+\bullet}$ – $3^{+\bullet}$) most of charge and spin are localized on sulfur (structures I and III in Figure 7).

Discussion

In the previous section, we have observed that two conformations (**a** and **b**), with different charge and spin distribution, are available for the radical cations $1^{+\bullet}$ – $3^{+\bullet}$ and $7^{+\bullet}$. At variance the two conformations for $4^{+\bullet}$ are both of the **b** type. The peculiarity of the **b** type conformations common to all radical cations is that they present the C–S bond perpendicular to the ring of the cumyl moiety and exhibit a substantial delocalization of SOMO in both rings. It seems reasonable to suggest that the **b** conformation is the most suitable one for the C–S bond cleavage as the empty carbon p orbital formed in the cleavage is perfectly suited for an efficient overlap with the π system (stereoelectronic effect) in the formed cumyl carbocation. Moreover, in this conformation the C–S bond is significantly longer than in the **a** conformation. We will therefore discuss the kinetic data in Table 2 by assuming that the **b** conformation is that undergoing C–S bond cleavage.³⁴

By considering first the series $1^{+\bullet}$ – $4^{+\bullet}$, where the radical cations differ only for the nature of the *para* substituent in the

cumyl moiety, it can be immediately noted that the C–S bond cleavage rates are very little sensitive to the nature of the substituent. As expected, the rates increase by increasing the electron-donating power of the substituent, that is, increasing the stability of the formed carbocation, but on going from bromo to methoxy the increase in rate is only by a factor of 12.5. In term of BDFE, the 5.5 kcal/mol difference in BDFE between the most reactive $4^{+\bullet}$ and the least reactive $1^{+\bullet}$ is associated to a very small difference in ΔG^\ddagger (1.5 kcal/mol).

Looking for more substantial effects, we also studied the *p*-X-cumyl *p*-methoxyphenyl sulfide radical cations $5^{+\bullet}$ – $7^{+\bullet}$ hoping that with a more stable sulfur radical cation, the effect of the X substituent in the cumyl moiety on the C–S bond cleavage rate would be larger than that observed with $1^{+\bullet}$ – $4^{+\bullet}$. As expected, slower rates were observed with respect to $1^{+\bullet}$ – $4^{+\bullet}$, but unfortunately the decrease was such that it was possible to obtain reliable rates only for $7^{+\bullet}$, which precluded any comparison.

Anyway, we tried to treat the kinetic data for the fragmentation of radical cations $1^{+\bullet}$ – $4^{+\bullet}$, $7^{+\bullet}$ in terms of the Marcus equation, eq 2,³⁵ where ΔG^\ddagger is the activation free energy of the reaction, obtained by the rate constants in Table 2 via the Eyring equation (eq 3) with Z taken as $6 \times 10^{11} \text{ M}^{-1} \text{ s}^{-1}$.³⁶ ΔG° is the free energy variation in the same reaction (C–S BDFE given in Table 2), and λ is the reorganization energy required for the fragmentation process.

$$\Delta G^\ddagger = (\lambda/4)(1 + \Delta G^\circ/\lambda)^2 \quad (2)$$

$$\Delta G^\ddagger = RT \ln(Z/k_f) \quad (3)$$

Very rewardingly, a quite satisfactory fit of the experimental data to eq 2 was obtained, which is shown in Figure 8. From the nonlinear least-squares fitting a flat curve is obtained in accordance with the small influence of the BDFEs on the fragmentation rates described above. The λ value obtained from the fit ($43.7 \pm 3.1 \text{ kcal mol}^{-1}$, see also Figure S7 in Supporting Information) clearly indicates a quite high intrinsic barrier for the C–S bond cleavage reaction.

An interesting observation is that the very small sensitivity of the C–S bond cleavage rate to the stability of the formed carbocation for the sulfide radical cations displayed in Table 2 sharply contrasts with what is observed in the S_N1 solvolysis of sulfonium salts (eq 4, $R = \textit{tert}$ -alkyl, arylalkyl, or diarylalkyl)^{37,38} a reaction that formally strongly resembles the C–S bond cleavage in sulfur radical cations (eq 1), the only difference being that in eq 1 the leaving group is a sulfur radical, whereas in eq 4 it is a neutral sulfide. In this case, the stabilization of the incipient carbocation is the dominant factor affecting the solvolysis rate.³⁹ For example, in the solvolysis of X-substituted benzhydryldimethylsulfonium salts, the solvolysis rate in MeOH is

(33) A methoxy group in the cumyl ring is also present in $7^{+\bullet}$, and accordingly in this case too there is a significant enhancement of charge density in Ar_{cum} of the **b** conformation with respect to $1^{+\bullet}$ – $3^{+\bullet}$.

(34) In order to get an evaluation of the values of the interconversion barriers between **a** and **b** conformations, a conformational transition state was located (by using the keyword Opt=QST2) in the interconversion path between **a** and **b** conformations in radical cation $2^{+\bullet}$. The two barriers were found to be very low: 1.97 and 0.52 kcal/mol for the **a** \rightarrow **b** and **b** \rightarrow **a** conversion, respectively. Therefore it should no matter if the radical cation is predominantly formed in conformation **a** when this is the most stable conformation.

(35) Marcus, R. A. *Annu. Rev. Phys. Chem.* **1964**, *15*, 155.

(36) Ebersson, L. *Electron Transfer Reactions in Organic Chemistry*; Springer Verlag: Berlin Heidelberg, 1986; Chapter 3.

(37) Hine, J. B.; Golinkin, H. S. *Can. J. Chem.* **1963**, *41*, 3139–3142.

(38) Jurić, S.; Denegri, B.; Kronja, O. *J. Org. Chem.* **2010**, *75*, 3851–3854.

(39) The sensitivity of the solvolysis rate to the stability of the formed carbocation³⁷ was found to be very similar to that observed for the corresponding chlorides (very large $\rho^+ \approx -4.5$ for substituted *tert*-cumyl chlorides⁴⁰).

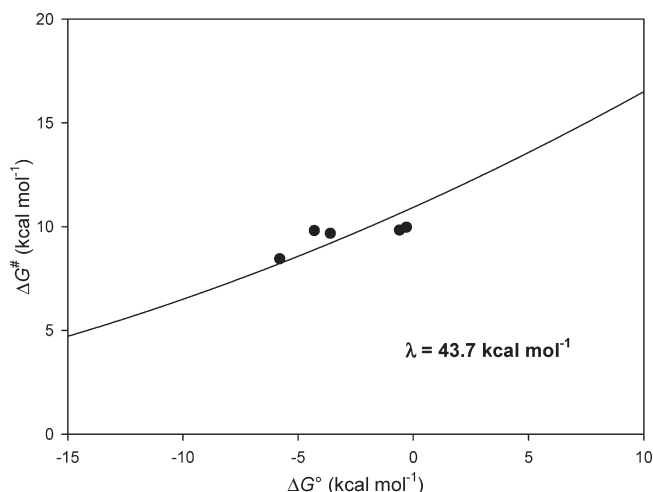
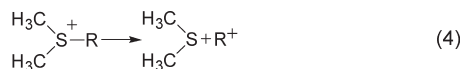


FIGURE 8. Diagram of ΔG^\ddagger vs ΔG° for the fragmentation reactions of radical cations $1^{+\bullet}$ – $4^{+\bullet}$, $7^{+\bullet}$. The solid circles correspond to the experimental values; the solid curve is calculated by nonlinear least-squares fit to eq 2.

accelerated by almost 30 times on passing from $X = \text{H}$ to $X = \text{Me}$.³⁸



We feel that a rationalization of the above difference may be traced back to the large differences in reactivity and in the initial state charge distribution of the two systems. In sulfonium salts, the solvolyses are very slow reactions, many orders of magnitude slower than the fragmentation of sulfur radical cations; moreover, in the initial state, the charge is almost completely located on the sulfur atom.³⁸ Thus, a late transition state with a well advanced state of C–S bond breaking can be predicted where a quite large amount of positive charge has been transferred from sulfur to the carbon, so determining a strong dependence of sulfonium salts solvolysis rates on the stability of the formed carbocation.

The situation is different in sulfur radical cations where, as already seen, a significant delocalization of spin and positive charge in the cumyl moiety is already present in the radical cation and the C–S BDFE is very low. It is therefore very probable that the transition state for the cleavage of the C–S bond is reached quite early along the reaction coordinate with very little further transfer of positive charge to the cumyl moiety. Hence, substituents that can stabilize the positive charge in the cumyl group should have a very small effect on the rate of C–S scission, as observed.

Another interesting comparison is also possible between the scission of the C–S bond in $4^{+\bullet}$ and the homolytic C–C bond cleavage in a *p*-methoxy-substituted bicumyl radical cation ($10^{+\bullet}$), a reaction studied in detail by Maslak and his group.⁴¹ As illustrated in Scheme 5, in both systems the positive charge is mainly (exclusively for $10^{+\bullet}$) located in the 4-methoxycumyl ring and the same carbocation is formed by C–S and C–C bond cleavage.

SCHEME 5. C–S and C–C Bond Cleavage of Radical Cations $4^{+\bullet}$ and $10^{+\bullet}$

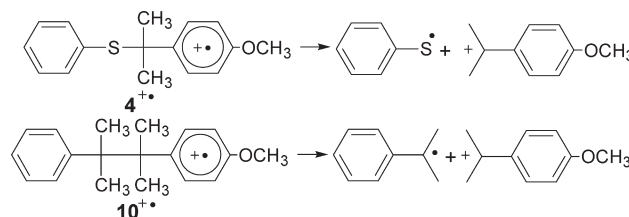


TABLE 5. Rate Constants (k_f), Activation Free Energies for Fragmentation Reactions (ΔG^\ddagger), and Bond Dissociation Free Energies (BDFEs) of Radical Cations $4^{+\bullet}$ and $10^{+\bullet}$

radical cations	k_f	ΔG^\ddagger ^a	BDFE ^a
$4^{+\bullet}$	$4.5 \times 10^5 \text{ s}^{-1}$	8.4	–5.1
$10^{+\bullet}$	$2.5 \times 10^7 \text{ s}^{-1}$ ^b	6.0 ^b	4.8 ^b

^akcal mol^{–1}. ^bref 41.

In Table 5 are reported the rate constants and the activation free energies of the fragmentation reactions in Scheme 5 together with the relative C–S and C–C bond dissociation free energies (BDFEs) for the two radical cations.

From the data reported in Table 5 it can be readily noted that the rate of C–S bond cleavage in $4^{+\bullet}$ is significantly lower than the rate of C–C bond cleavage in $10^{+\bullet}$, even though the former reaction is exergonic while the second process is endergonic. This leads to the conclusion that the C–S bond cleavage in cumyl aryl sulfide radical cations is intrinsically a much slower process than the C–C bond cleavage in bicumyl radical cations. Indeed, a λ value as low as 12 kcal mol^{–1} was determined for the C–C bond cleavage in the bicumyl radical cation,^{41,42} which should be compared with a λ for the C–S bond cleavage of 43.7 kcal mol^{–1}, obtained from the Marcus plot in Figure 8.

The kinetic barrier associated with the bond cleavage in an aromatic radical cation, should derive from the intramolecular nuclear and solvent reorganization attending the transfer of an electron from the σ orbital of the scissile bond to the aromatic π system. The above results indicate that the cost of this reorganization is significantly higher for the C–S than for the C–C bond cleavage. A tentative explanation might consider that whereas in $10^{+\bullet}$ all of the charge is localized in the methoxylated ring and remains in that ring after the C–C bond cleavage, in $4^{+\bullet}$ a substantial amount (almost half) of charge is also localized in the ArS moiety of the radical cation, as indicated by DFT calculations. This implies that such a charge has to be transferred to the cumyl moiety in the final products. Thus, the extent of the reorganization should be much larger for the C–S bond cleavage in $4^{+\bullet}$ than for the C–C bond cleavage in $10^{+\bullet}$, which certainly should

(42) It should be pointed out, however, that the difference in λ between C–C and C–S bond cleavage might be somewhat lower than that resulting from the above figures since it is known that DFT calculations may underestimate the values of the BDEs of the C–S bond in the neutral substrates from which the BDFE energy for $4^{+\bullet}$ has been obtained by the thermochemical cycle. However, even with a C–S BDE for **4** that is 6–8 kcal mol^{–1} larger than that resulting from DFT calculations, the difference in the kinetic barrier between C–C and C–S bond cleavage in aromatic radical cations would remain very significant. For example the fit in Figure 8 using 8 kcal mol^{–1} more positive ΔG° values leads to a lower λ value (27.0 kcal mol^{–1}), which is however still much higher than the 12 kcal mol^{–1} calculated for the C–C bond cleavage reaction. On the other hand, C–C bond cleavage would remain 2 kcal mol^{–1} more endergonic than C–S bond cleavage.

(40) Okamoto, Y.; Inukai, T.; Brown, H. C. *J. Am. Chem. Soc.* **1958**, *80*, 4972–4976.

(41) Maslak, P.; Vallombroso, T. M.; Chapman, W. H.; Narvaez, J. N. *Angew. Chem., Int. Ed. Engl.* **1994**, *33*, 73–75.

significantly contribute to making the kinetic barrier for the former cleavage higher than for the second. In addition the solvent reorganization too should be larger for the C–S than the C–C bond cleavage as the former entails a larger degree of charge transfer from ArS to the cumyl moiety.

Conclusions

C–S Bond cleavage in aryl 1-methyl-1-arylethyl sulfide radical cations $1^{+\bullet}$ – $7^{+\bullet}$ is an exergonic or almost isergonic process leading to cumyl cations and arylsulfenyl radicals, characterized by a relatively low reaction rate (10^4 – 10^5 s $^{-1}$) and by only a modest increase of the fragmentation rate constants by increasing the stability of the formed cumyl carbocation, i.e., as the C–S bond dissociation free energies (BDFEs) become more negative. These results have been rationalized by considering (DFT calculations) that the conformation most suitable for C–S bond cleavage (C–S bond almost collinear with the π system of the cumyl ring) allows that a significant fraction of charge and spin is distributed in the ArS ring and in the cumyl ring. Thus, little further accumulation of positive charge at the cumyl carbon should occur at the transition state of the C–S scission reaction. The fact that charge and spin are delocalized among the two rings of the radical cations may also be responsible for the large reorganization energy ($\lambda = 43.7$ kcal mol $^{-1}$) estimated for the C–S bond scission by the Marcus equation, which makes such a scission intrinsically much slower than C–C bond cleavage in bicumyl radical cations, a reaction that also leads to cumyl carbocations.

Experimental Section

Steady State Photolysis. Photooxidation reactions were carried out in a photoreactor equipped with 4 lamps (360 nm; 14 W each). A 2 mL solution containing the substrate **1**–**7** (1.0×10^{-2} M) and MeOP $^+$ (5×10^{-3} M) in N $_2$ -saturated CD $_3$ CN was placed in a quartz cell and irradiated with two phosphor-coated fluorescent lamps emitting at 355 ± 15 nm. The light intensity (ca. 3×10^{15} photons s $^{-1}$) was measured by potassium ferric oxalate actinometry. An internal standard (bibenzyl)

was added and the mixtures were analyzed by ^1H NMR, GC, and GC–MS. The following products were identified by comparison with authentic specimens: 2-phenyl-2-propanol, 2-(4-methoxyphenyl)-2-propanol, 2-(4-methylphenyl)-2-propanol, 2-(4-bromophenyl)-2-propanol, bis(4-methoxyphenyl) disulfide, diphenyl disulfide, protonated phenanthridine, and methanol. 2,4-Bis(4-methoxyphenyl)-4-methyl-1-pentene and (*E*)-2,4-bis(4-methoxyphenyl)-4-methyl-2-pentene were identified by comparison of the ^1H NMR and GC–MS data with those reported in the literature.¹² The photoproducts were quantified by GC and ^1H NMR. The material balance was always satisfactory (>90%). Blank experiment, carried out by irradiating the solutions in the absence of MeOP $^+$, did not show in all cases product formation.

Laser Flash Photolysis. Excitation wavelength of 355 nm (Nd:YAG laser, Continuum, third harmonic, pulse width ca. 7 ns and energy <3 mJ per pulse) was used in nanosecond flash photolysis experiments. The transient spectra were obtained by a point-to-point technique, monitoring the change of absorbance (ΔA) after the laser flash at intervals of 5–10 nm over the spectral range 300–800 nm, averaging at least 10 decays at each wavelength. Nitrogen was bubbling through the solution. All measurements were carried out at 22 ± 2 °C unless otherwise indicated. The experimental error was $\pm 10\%$.

Acknowledgment. Financial support from the Ministero dell'Istruzione, dell'Università e della Ricerca (MIUR) is gratefully acknowledged.

Supporting Information Available: Starting materials, time-resolved absorption spectra after LFP of the MeOP $^+$ /**1**–**2**, **5**–**7** systems; cyclic voltammetry; C–S BDFEs of radical cations $1^{+\bullet}$ – $7^{+\bullet}$; degree of planarity of the cumyl carbon bonded to the S atom in neutral sulfides **1**–**4**, **7** and in sulfide radical cations $1^{+\bullet}$ – $4^{+\bullet}$, $7^{+\bullet}$; diagram of ΔG^\ddagger vs ΔG° for the fragmentation reactions of radical cations $1^{+\bullet}$ – $4^{+\bullet}$, $7^{+\bullet}$ with error limits; Cartesian Coordinates, energies, ZPVE from DFT calculations for neutral sulfides **1**–**7**, for cumyl and arylsulfenyl radicals and for radical cations $1^{+\bullet}$ – $4^{+\bullet}$, $7^{+\bullet}$; $2^{+\bullet}$ – $4^{+\bullet}$, $7^{+\bullet}$ conformers at the minimum of energy; NPA Charges and Mulliken spin densities for radical cation $1^{+\bullet}$ – $4^{+\bullet}$, $7^{+\bullet}$. This material is available free of charge via the Internet at <http://pubs.acs.org>.